Magnetic ordering, orbital ordering, and resonant x-ray scattering in perovskite titanates

S. Ishihara
Department of Applied Physics, University of Tokyo, Tokyo 113-8656, Japan

T. Hatakeyama and S. Maekawa
Institute for Materials Research, Tohoku University, Sendai 980-8577, Japan
(Received 8 July 2001; published 24 January 2002)

The effective Hamiltonian for perovskite titanates is derived by taking into account the threefold degeneracy of t_{2g} orbitals and the strong electron-electron interactions. The magnetic and orbital ordered phases are studied in the mean-field approximation applied to the effective Hamiltonian. A large degeneracy of the orbital states in the ferromagnetic phase is found in contrast to the case of the doubly degenerate e_g orbitals. Lifting of this orbital degeneracy due to lattice distortions and spin-orbit coupling is examined. A general form for the scattering cross section of the resonant x-ray scattering is derived and is applied to the recent experimental results in $YTiO_3$. The spin wave dispersion relation in the orbital ordered $YTiO_3$ is also studied.

DOI: 10.1103/PhysRevB.65.064442 PACS number(s): 75.10.−b, 71.10.−w, 78.70.−g, 71.30.+h

I. INTRODCUTION

Since the discovery of layered superconducting cuprates $La_{2-x}Sr_xCuO_4$, studies of electronic structures of transition-metal oxides are revived from the modern view point of electron correlation.[1] Perovskite titanates $R_{1-x}A_xTiO_3$ are one of the prototypical three-dimensional materials which show the Mott transition and anomalous metallic states at a vicinity of the transition. Here, R and A indicate the trivalent and divalent cations, respectively. The end compounds $RTiO_3$, where a nominal valence of all Ti ions is $3+$, are recognized to be Mott insulators. A mismatch of the ionic radius in the pseudocubic structure induces the $GdFeO_3$-type lattice distortion, i.e., a tilting of a TiO_6 octahedron.[2] The electronic structure of $RTiO_3$ systematically changes with a kind of the rare-earth ion R;[1,3,4] a large distorted $YTiO_3$ shows a ferromagnetic ordering at 29 K. The saturated magnetic moment is 0.84,[5] which is close to the expected value from $S=1/2$, and a definite optical gap is observed to be about 2 eV.[6,7] On the contrary, the insulating character of the less distorted $LaTiO_3$ is more marginal than $YTiO_3$; a staggered magnetic moment for the G-type antiferromagnetic (AF) state is less than one half of the expected value[3] and an insulating gap is smaller than 0.5 eV.[6,8] By doping $RTiO_3$ with holes, the system undergoes the metal-insulator transition and exhibits several unconventional metallic characters ascribed to the electron correlation,[9–11] as well as $La_{2-x}Sr_xCuO_4$.

One of the remarkable discrepancies in perovskite titanates from layered superconducting cuprates is that the orbital degree of freedom survives in titanates; the electron configuration of Ti^{3+} is d^1 where the three t_{2g} orbitals, i.e., d_{xy}, d_{yz}, and d_{zx} orbitals, are degenerate under the cubic crystalline field. Thus, this ion has a degree of freedom which indicates an occupied orbital by an electron. The intensive and extensive studies of the orbital degree of freedom have been carried out recently in colossal magnetoresistive (CMR) manganites[12] where a Mn^{3+} ion has doubly degenerate e_g orbitals. Here, it is widely believed that observed dramatic phenomena such as CMR are caused by strong interplay between spin, charge, and orbital, as well as lattice. In comparison with manganites, there exist following characteristics in the orbital degree of freedom in titanates: (1) there is a threefold degeneracy of the t_{2g} orbitals, (2) an electron hopping between nearest-neighboring (NN) different orbitals is prohibited in a cubic crystal structure, (3) the spin-orbit (LS) coupling is possible to be relevant, and (4) the cooperative Jahn-Teller (JT) effect is weak.[2] Actually, some theoretical and experimental studies of perovskite titanates have been done from the view point of the orbital degree of freedom.[13–22] In addition, the resonant x-ray scattering (RXS) was applied to $RTiO_3$ very recently[18,22] and the orbital ordering was successfully observed in $YTiO_3$.[22] The systematic studies by utilizing this experimental method are expected to clarify roles of the orbital degree of freedom in the Mott transition and the several unconventional phenomena observed in titanates.

In this paper, the effective Hamiltonian for the electronic structures in perovskite titanates is derived and the spin and orbital structures in $RTiO_3$ are studied in the mean field approximation. The derived Hamiltonian corresponds to the tJ model in superconducting cuprates[23] and the spin-orbital model for CMR manganites,[24] and is applicable to a wide range of doped and undoped titanates. In particular, we focus on roles of the threefold degeneracy in the t_{2g} orbitals. It is shown that the orbital degeneracy of the ground state is more significant than that in the e_g orbital case. A general form for the scattering cross section of RXS is derived and is applied to the recent experimental results in $YTiO_3$.[22] Roles of the orbital on the spin wave dispersion relation in $YTiO_3$ are also discussed.

II. EFFECTIVE HAMILTONIAN

We start with the tight-binding Hamiltonian in a three dimensional lattice consisting of Ti ions. Three t_{2g} orbitals d_{xy}, d_{yz} and d_{zx} and the intra-atomic Coulomb interactions

are considered in each Ti ion. The Hamiltonian is

$$\mathcal{H}=\sum_{\langle ij\rangle\gamma\gamma'\sigma}(t_{ij}^{\gamma\gamma'}d_{i\gamma\sigma}^{\dagger}d_{j\gamma'\sigma}+\text{H.c.})+U\sum_{i\gamma}n_{i\gamma\uparrow}n_{i\gamma\downarrow}+U'\frac{1}{2}\sum_{i\gamma\neq\gamma'}n_{i\gamma}n_{i\gamma'}+I\sum_{i\gamma>\gamma'\sigma\sigma'}d_{i\gamma\sigma}^{\dagger}d_{i\gamma'\sigma'}^{\dagger}d_{i\gamma\sigma'}d_{i\gamma'\sigma}+I\sum_{i\gamma\neq\gamma'}d_{i\gamma\uparrow}^{\dagger}d_{i\gamma\downarrow}^{\dagger}d_{i\gamma'\downarrow}d_{i\gamma'\uparrow}, \tag{1}$$

where $d_{i\gamma\sigma}^{\dagger}$ creates a t_{2g} electron at site i with spin σ $(=\uparrow,\downarrow)$ and orbital $\gamma(=xy,yz,zx)$. U and U' are the intraorbital and interorbital Coulomb interactions, respectively, and I is the exchange interaction. In an isolated ion, these interactions are represented by the Racah parameters as $U=A+4B+3C, U'=A-2B+C$ and $I=3B+C$, and a relation $U=U'+2I$ is satisfied. $t_{ij}^{\gamma\gamma'}$ is the hopping integral between site i and its NN site j with orbitals γ and γ', respectively. In a simple cubic lattice, the hopping integral is diagonal and one of the diagonal components is zero. For a Ti-Ti bond in a direction $l(=x,y,z)$, two orbitals, which have a finite hopping integral $t_{ij}^{\gamma\gamma}$, are termed active orbitals denoted by a_l and b_l, and one with no hopping integral is termed an inactive orbital denoted by c_l. For example, $(a_x,b_x,c_x)=(zx,xy,yz)$. $t_{ij}^{\gamma\gamma'}$ is simply expressed in this case as

$$t_{ij}^{\gamma\gamma'}=t\delta_{\gamma\gamma'}(\delta_{\gamma a_l}+\delta_{\gamma b_l}). \tag{2}$$

The $GeFeO_3$-type lattice distortion breaks this relation as discussed in Sec. III.

Since the Coulomb interactions U and U' are larger than the hopping integral in titanates,[25] the effective Hamiltonian is derived by perturbational calculation with respect to the hopping integral. The Hamiltonian is

$$\mathcal{H}=\mathcal{H}_t+\mathcal{H}_J, \tag{3}$$

where the first and second terms correspond to the so-called t and J terms in the tJ model, respectively. The t term is given by

$$\mathcal{H}_t=\sum_{\langle ij\rangle\gamma\gamma'\sigma}t_{ij}^{\gamma\gamma'}\tilde{d}_{i\gamma\sigma}^{\dagger}\tilde{d}_{j\gamma'\sigma}+\text{H.c.}, \tag{4}$$

where $\tilde{d}_{i\gamma\sigma}[=d_{i\gamma\sigma}\Pi_{(\gamma'\sigma')\neq(\gamma\sigma)}(1-d_{i\gamma'\sigma'}^{\dagger}d_{i\gamma'\sigma'})]$ excludes multioccupied states of electrons at site i. The J term is classified by the point symmetry of the intermediate electronic states, i.e., d^2 states. In the case where Eq. (2) is satisfied, the Hamiltonian is

$$\mathcal{H}_J=\mathcal{H}_{T_1}+\mathcal{H}_{T_2}+\mathcal{H}_E+\mathcal{H}_{A_1}, \tag{5}$$

with

$$\mathcal{H}_{T_1}=-J_{T_1}\sum_{\langle ij\rangle}\left(\frac{3}{4}n_in_j+\vec{S}_i\cdot\vec{S}_j\right)(B^l-C^l+D^l), \tag{6}$$

$$\mathcal{H}_{T_2}=-J_{T_2}\sum_{\langle ij\rangle}\left(\frac{1}{4}n_in_j-\vec{S}_i\cdot\vec{S}_j\right)(B^l+C^l+D^l), \tag{7}$$

$$\mathcal{H}_E=-J_E\sum_{\langle ij\rangle}\left(\frac{1}{4}n_in_j-\vec{S}_i\cdot\vec{S}_j\right)\left(\frac{2}{3}A^l-\frac{2}{3}C'^l\right), \tag{8}$$

$$\mathcal{H}_{A_1}=-J_{A_1}\sum_{\langle ij\rangle}\left(\frac{1}{4}n_in_j-\vec{S}_i\cdot\vec{S}_j\right)\left(\frac{1}{3}A^l+\frac{2}{3}C'^l\right). \tag{9}$$

Prefactors are given by $J_{T_1}=t^2/(U'-I), J_{T_2}=t^2/(U'+I), J_E=t^2/(U-I)$ and $J_{A_1}=t^2/(U+2I)$. By using the relation $U=U'+2I$, we obtain $J_{T_2}=J_E$. $n_i(=\Sigma_{\sigma\gamma}d_{i\gamma\sigma}^{\dagger}d_{i\gamma\sigma})$ is the number operator and $\vec{S}_i$ is the spin operator given by

$$\vec{S}_i=\frac{1}{2}\sum_{\gamma\sigma\sigma'}d_{i\gamma\sigma}^{\dagger}\vec{\sigma}_{\sigma\sigma'}d_{i\gamma\sigma'}. \tag{10}$$

A^l, B^l, C^l, C'^l, and D^l are the orbital parts of the Hamiltonian represented by the eight orbital operators $O_{\Gamma\gamma}$ where Γ denotes an irreducible representation in the O_h group and γ classifies the bases of the irreducible representation. To represent $O_{\Gamma\gamma}$, let us introduce the Gell-Mann matrices which are generators of the SU(3) algebra[26]

$$\lambda_1=\begin{pmatrix}0&1&0\\1&0&0\\0&0&0\end{pmatrix},\quad \lambda_2=\begin{pmatrix}0&-i&0\\i&0&0\\0&0&0\end{pmatrix}, \tag{11}$$

$$\lambda_3=\begin{pmatrix}-1&0&0\\0&1&0\\0&0&0\end{pmatrix},\quad \lambda_4=\begin{pmatrix}0&0&1\\0&0&0\\1&0&0\end{pmatrix}, \tag{12}$$

$$\lambda_5=\begin{pmatrix}0&0&i\\0&0&0\\-i&0&0\end{pmatrix},\quad \lambda_6=\begin{pmatrix}0&0&0\\0&0&1\\0&1&0\end{pmatrix}, \tag{13}$$

$$\lambda_7=\begin{pmatrix}0&0&0\\0&0&-i\\0&i&0\end{pmatrix},\quad \lambda_8=\frac{1}{\sqrt{3}}\begin{pmatrix}1&0&0\\0&1&0\\0&0&-2\end{pmatrix}. \tag{14}$$

We define the orbital operators as

$$O_{i\Gamma\gamma}=\frac{-1}{\sqrt{2}}\sum_{\sigma\alpha\beta}d_{i\alpha\sigma}^{\dagger}(\lambda_l)_{\alpha\beta}d_{i\beta\sigma}, \tag{15}$$

where $(\Gamma\gamma;l)=(Eu;8),(Ev,3),(T_2x;6),(T_2y;4),(T_2z;1),(T_1x;7),(T_1y;5)$, and $(T_1z;2)$. The operators $O_{iE\gamma}$ and $O_{iT_2\gamma}$ describe the electric quadrupole moments and $O_{iT_1\gamma}$ describes the magnetic dipole moment. By utilizing the above operators, we obtain

$$A^l=2\left(\frac{2}{3}-\sqrt{\frac{2}{3}}O_{iEu}^l\right)\left(\frac{2}{3}-\sqrt{\frac{2}{3}}O_{jEu}^l\right)+4O_{iEv}^lO_{jEv}^l, \tag{16}$$

$$B^l=\left(\frac{2}{3}-\sqrt{\frac{2}{3}}O^l_{iEu}\right)\left(\frac{2}{3}-\sqrt{\frac{2}{3}}O^l_{jEu}\right)-2O^l_{iEv}O^l_{jEv}, \tag{17}$$

$$C^l=2(O_{iT_2l}O_{jT_2l}+O_{iT_1l}O_{jT_1l}), \tag{18}$$

$$C'^l=2(O_{iT_2l}O_{jT_2l}-O_{iT_1l}O_{jT_1l}) \tag{19}$$

$$D^l=\left(\frac{1}{3}+\sqrt{\frac{2}{3}}O^l_{iEu}\right)\left(\frac{2}{3}-\sqrt{\frac{2}{3}}O^l_{jEu}\right)+\left(\frac{2}{3}-\sqrt{\frac{2}{3}}O^l_{iEu}\right)\times\left(\frac{1}{3}+\sqrt{\frac{2}{3}}O^l_{jEu}\right), \tag{20}$$

where $O^l_{iE\gamma}$'s are given by

$$\begin{pmatrix}O^l_{iEu}\\ O^l_{iEv}\end{pmatrix}=\begin{pmatrix}\cos\frac{2\pi}{3}m_l & \sin\frac{2\pi}{3}m_l\\ -\sin\frac{2\pi}{3}m_l & \cos\frac{2\pi}{3}m_l\end{pmatrix}\begin{pmatrix}O_{iEu}\\ O_{iEv}\end{pmatrix}, \tag{21}$$

with $m_l=(1,2,3)$ for $l=(x,y,z)$. It is worth rewriting the orbital parts of the Hamiltonian from the view point of the active and inactive orbitals; we introduce the pseudospin operator with the quantum number 1/2 for a bond along a direction l

$$\vec{T}^l_i=\frac{1}{2}\sum_{\gamma,\gamma'=(a_l,b_l),\sigma} d^\dagger_{i\gamma\sigma}\vec{\sigma}_{\gamma\gamma'}d_{i\gamma'\sigma}, \tag{22}$$

with $\vec{\sigma}$ being the Pauli matrices, and the number operator $n_{i\gamma_l}=\Sigma_\sigma d^\dagger_{i\gamma_l\sigma}d_{i\gamma_l\sigma}$ for $\gamma_l=(a_l,b_l,c_l)$. The orbital parts of the Hamiltonian are rewritten as

$$A^l=4(n_{ia_l}n_{ja_l}+n_{ib_l}n_{jb_l}), \tag{23}$$

$$B^l=2(n_{ia_l}n_{jb_l}+n_{ib_l}n_{ja_l}), \tag{24}$$

$$C^l=4(T^l_{ix}T^l_{jx}+T^l_{iy}T^l_{jy}), \tag{25}$$

$$C'^l=4(T^l_{ix}T^l_{jx}-T^l_{iy}T^l_{jy}), \tag{26}$$

$$D^l=n_{ic_l}(n_{ja_l}+n_{jb_l})+(n_{ia_l}+n_{ib_l})n_{jc_l}. \tag{27}$$

We note that $\vec{T}^l_i$'s with different l are not independent with each other. These simple expressions result from the diagonal form in the hopping integral under which an electron number of each orbital is conserved. Schematic pictures of representative exchange processes for A^l,B^l,C^l, and D^l are shown in Fig. 1.

A similar model Hamiltonian with Eq. (5) was derived in Ref. 27, although the intra-atomic exchange interaction I is assumed to be zero. As shown in the next section, this condition corresponds to a critical point in the phase diagram. Also, a similar model with $I=0$ is represented by the pseudospin operators T^l_i [Eq. (22)] in Ref. 19. In a model Hamiltonian derived in Ref. 20, two of the three t_{2g} orbitals are taken into account.

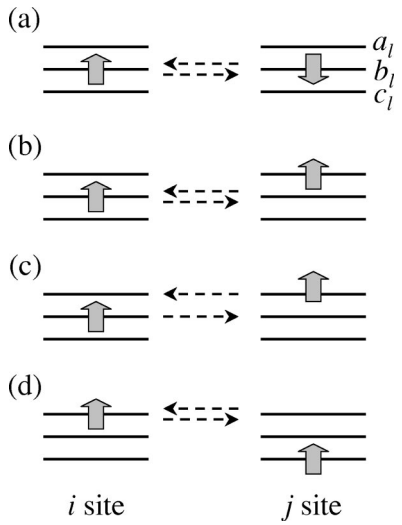

FIG. 1. Schematic pictures of representative virtual exchange processes for the terms (a) A^l, (b) B^l, (c) C^l, and (d) D^l defined in Eqs. (16), (17), (18), and (20), respectively. a_l and b_l are the active orbitals and c_l is the inactive orbital (see text).

III. SPIN AND ORBITAL STATES

The effective Hamiltonian is applied to $R\mathrm{TiO_3}$ where a valence of all Ti ion is $3+$. Consider a hypothetical-cubic lattice consisting of Ti ions, instead of the actual crystal lattice of $R\mathrm{TiO_3}$. The mean-field approximation at zero temperature is applied to the Hamiltonian and the four kinds of spin and orbital ordered states are considered; a uniform spin (orbital) state termed F and three staggered spin (orbital) states termed A-AF, C-AF, and G-AF. The periodicities of these orderings are characterized by the momentum $(000),(00\pi),(\pi\pi0)$, and $(\pi\pi\pi)$, respectively. $\langle S_{iz}\rangle\times(=\pm1/2)$ is adopted to be a spin order parameter and, the orbital order parameters $\langle O_{i\Gamma\gamma}\rangle$ are calculated by the orbital wave function at site i

$$|\psi_i\rangle=C_{ixy}|d_{ixy}\rangle+C_{iyz}|d_{iyz}\rangle+C_{izx}|d_{izx}\rangle. \tag{28}$$

The order parameters are optimized numerically to obtain the lowest energy.

In Fig. 2, the magnetic and orbital phase diagram is presented as a function of $R_J\equiv J_{A_1}/J_{T_1}$. The relation $J_{T_2}/J_{T_1}=5R_J/(2+3R_J)$ derived from the condition $U=U'+2I$ is used. Although a value of R_J is smaller than one in actual compounds, the calculated results in the region of $R_J>1$ are also shown for comparison. In the region of $R_J<1$, the F spin state and the G-AF orbital ordered state are realized. The wave functions in the A and B orbital sublattices are given by

$$|\psi_A\rangle=|d_\alpha\rangle,$$

$$|\psi_B\rangle=\cos\theta|d_\beta\rangle+\sin\theta e^{i\phi}|d_\gamma\rangle, \tag{29}$$

respectively, with any values of $\theta\in[0,\pi]$ and $\phi\in[0,2\pi]$, and $(\alpha,\beta,\gamma)=(xy,yz,zx),(yz,zx,xy),(zx,xy,yz)$. There is a large continuous degeneracy in the orbital state; any linear

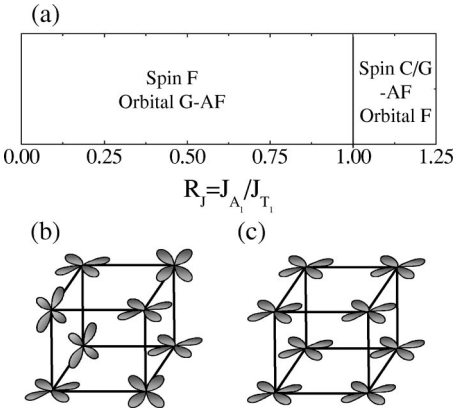

FIG. 2. (a) The spin and orbital phase diagram as a function of $R_J(\equiv J_{A_1}/J_{T_1})$. Schematic pictures of the representative orbital ordered states for $R_J<1$ and $R_J>1$ are shown in (b) and (c), respectively.

combinations of $|d_\beta\rangle$ and $|d_\gamma\rangle$ are degenerate in the sublattice B. This is generalized to the states

$$|\psi_{i_A}\rangle=|d_\alpha\rangle,$$

$$|\psi_{j_B}\rangle=\cos\theta_{j_B}|d_\beta\rangle+\sin\theta_{j_B}e^{i\phi_{j_B}}|d_\gamma\rangle, \tag{30}$$

where $i_A(j_B)$ indicates the $i(j)$-th site in the $A(B)$ orbital sublattice. θ_{j_B} and ϕ_{j_B} at each site are taken independently, because the Hamiltonian includes the interactions between the NN sites. In order to understand this state in more detail, let us consider the hopping integral between the NN occupied orbitals defined by

$$\tau_{ij}=\left\langle \psi_i\left|\sum_{\langle ij\rangle\gamma\gamma'\sigma} t_{ij}^{\gamma\gamma'}\tilde{d}_{i\gamma\sigma}^{\dagger}\tilde{d}_{j\gamma'\sigma}+\text{H.c.}\right|\psi_j\right\rangle. \tag{31}$$

τ_{ij}'s are zero for all bonds in this orbital ordered state. Therefore, the exchange processes denoted by A^l [Eq. (16)] do not occur (see Fig. 1), and the ferromagnetic interaction is dominant. It is worth comparing the present results with those in the system where the doubly degenerate e_g orbitals, i.e., the $d_{3z^2-r^2}$ and $d_{x^2-y^2}$ orbitals, exist. Here, the effective Hamiltonian corresponding to Eq. (5) is expressed by the spin operator $\vec{S}_i$ and the pseudospin operator for the orbital degree of freedom $\vec{T}_i$ with the quantum number 1/2.[24,28] The orbital state in the ferromagnetic phase obtained by the mean-field approximation is the G-AF orbital state where the wave functions are given by

$$|\psi_A\rangle=\cos\left(\frac{\theta}{2}\right)|d_{3z^2-r^2}\rangle+\sin\left(\frac{\theta}{2}\right)|d_{x^2-y^2}\rangle,$$

$$|\psi_B\rangle=-\sin\left(\frac{\theta}{2}\right)|d_{3z^2-r^2}\rangle+\cos\left(\frac{\theta}{2}\right)|d_{x^2-y^2}\rangle, \tag{32}$$

for any value of $\theta\in[0,2\pi]$.[29] This is also a staggered orbital ordered state with a continuous degeneracy. However, remarkable differences between the t_{2g} and e_g cases exist. (1) The hopping integrals between the occupied orbitals τ_{ij} are finite in the e_g case and depend on θ. Thus, the generalization of the orbital ordered state, as seen in the t_{2g} case [from Eqs. (29) and (30)], is impossible. That is, the orbital degeneracy in the ground state is more remarkable in the t_{2g} case. This is because a number of the orbital degree of freedom is larger in this case. (2) The orbital wave functions with complex coefficients are not included in the e_g case. This is because the effective Hamiltonian for the e_g electron is represented by the operators T_x and T_z, unlike T_y which breaks the time reversal symmetry. In the region of $R_J>1$ in Fig. 2, there is no continuous orbital degeneracy. The C-AF and G-AF spin states are realized associated with the F orbital state with $|\psi\rangle=|d_\alpha\rangle$ for $\alpha=(xy,yz,zx)$. The point $R_J=1$, i.e., $I=0$, is a critical point in the phase diagram where degeneracy of the spin and orbital states are significant. It is supposed that R_J for $R\text{TiO}_3$ is about $0.2\sim0.4$,[13] although there is a large ambiguity in an estimation of I.

We next examine how this large continuous orbital degeneracy is lifted by the following three effects observed in $R\text{TiO}_3$: the GdFeO_3-type lattice distortion, the JT-type distortion in a TiO_6 octahedron and the LS coupling. The GdFeO_3-type lattice distortion bends a Ti-O-Ti bond. The simple form of the hopping integral in Eq. (2) is not valid and $t_{ij}^{\gamma\gamma'}$ for any pairs of γ and γ' are finite. We calculate all components of the hopping integral $t_{ij}^{\gamma\gamma'}$ for the crystal structures in YTiO_3 and LaTiO_3 by the Slater-Koster formula.[30] The most remarkable changes are found in the hopping integrals between the different active orbitals $t_{ij}^{a_l b_l}$. This is because the GdFeO_3-type distortion induces a σ bond between the $d_{a_l}(d_{b_l})$ orbital and the $2p_l$ orbital at the NN O site. We simulate this distortion by introducing a new term in the hopping integral as

$$t_{ij}^{\gamma\gamma'}=(t_\pi\delta_{\gamma\gamma'}+s_l t_\sigma\delta_{\gamma\neq\gamma'})(\delta_{\gamma a_l}+\delta_{\gamma b_l}), \tag{33}$$

where the sign of the transfer integral $s_l=\pm1$ depends on the direction l and a parameter $R_t=t_\sigma/t_\pi$ is interpreted to be an increasing function of this distortion. A value of R_t for YTiO_3 is estimated to be about $0.5\sim1$. The effective Hamiltonian including the GdFeO_3-type distortion, the JT-type distortion and the LS coupling is given by

$$\mathcal{H}=\tilde{\mathcal{H}}_J+\mathcal{H}_{JT}+\mathcal{H}_{LS}, \tag{34}$$

where t term H_t is neglected. The first term is the modified J term including the GdFeO_3-type distortion and its explicit form is presented in the Appendix A. The second term is for the JT coupling

$$\mathcal{H}_{\text{JT}}=g_E\sum_{i\gamma=u,v}O_{iE\gamma}Q_{iE\gamma}+g_{T_2}\sum_{i\gamma=x,y,z}O_{iT_2\gamma}Q_{iT_2\gamma}, \tag{35}$$

where $Q_{\Gamma\gamma}$'s are the normal coordinates of the oxygen displacements in a TiO_6 octahedron with the symmetry $\Gamma\gamma$, and g_Γ's are the coupling constants. The last term is for the LS coupling denoted by

$$\mathcal{H}_{\text{LS}}=\lambda_{\text{LS}}\sum_{i\gamma=x,y,z}S_{i\gamma}O_{iT_1\gamma}. \tag{36}$$

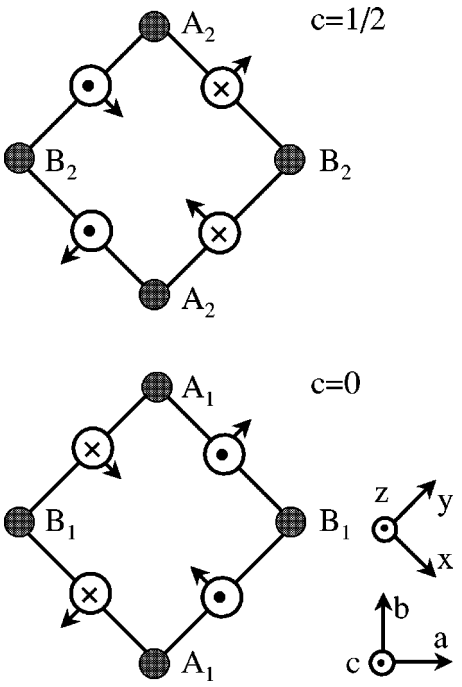

FIG. 3. A schematic picture of the crystal structure of $R\mathrm{TiO_3}$. Filled and open circles indicate Ti and O ions, respectively, and A_1, A_2, B_1, and B_2 denote Ti sites in a unit cell. Arrows indicate displacements of O ions in the ab plane, and crosses and dots in the O ions indicate the displacement along the $+c$ and $-c$ directions, respectively.

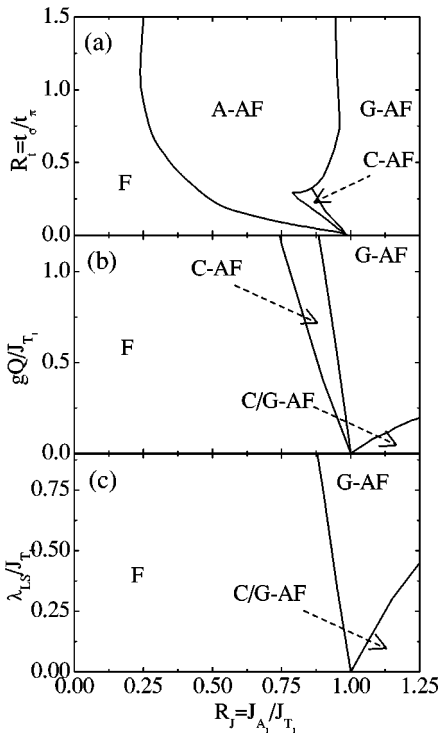

FIG. 4. The magnetic phase diagrams as functions of R_J and (a) a ratio between the hopping integrals $R_t = t_\sigma / t_\pi$ caused by the $\mathrm{GdFeO_3}$-type lattice distortion, (b) the JT-type lattice distortion gQ, and (c) LS coupling λ_{LS}. Other parameter values are chosen to be $\lambda_{\mathrm{LS}} = R_t = 0$ in (a), $gQ = \lambda_{\mathrm{LS}} = 0$ in (b), and $gQ = R_t = 0$ in (c).

The corrections for the effective Hamiltonian in Eq. (34) are of the order of $O(g_\Gamma t^2/U^2)$ and $O(\lambda_{\mathrm{LS}} t^2/U^2)$. In the mean field calculation, an orthorhombic unit cell with the $Pbnm$ space group is adopted. Four Ti ions in a unit cell are termed A_1, A_2, B_1, and B_2 (see Fig. 3) and the orbital states at these sites are considered independently. As for the JT-type distortion, $Q_{T_{2y}}$ and $(-1/2)Q_{Eu} + (\sqrt{3}/2)Q_{Ev} (\equiv Q_{E3x^2-r^2})$ are dominant at site A_1 in $\mathrm{YTiO_3}$. Thus, we assume in this calculation that $|g_{T_2}| Q_{A_1 T_{2y}} = |g_E| Q_{A_1 E 3x^2-r^2} (\equiv gQ)$ and other components are zero. The JT-type distortions at other sites are introduced by considering the $Pbnm$ space group.

The phase diagrams with including the $\mathrm{GdFeO_3}$-type lattice distortion, the JT-type distortion and the LS coupling are presented in Figs. 4(a), 4(b), and 4(c), respectively. In all phase diagrams, the large orbital degeneracy is lifted and a region of the ferromagnetic phase shrinks. This result implies that the high symmetry in the orbital space is favorable for the ferromagnetic spin ordering. The characteristics of the each phase diagram are summarized as follows. (1) By introducing the $\mathrm{GdFeO_3}$-type lattice distortion, the orbital degeneracy is partially lifted and one of orbital ordered states in the ferromagnetic phase is given by $|\psi_{A_1}\rangle = 0.71|d_{xy}\rangle + 0.71|d_{yz}\rangle$, $|\psi_{B_1}\rangle = 0.38|d_{xy}\rangle - 0.35|d_{yz}\rangle + 0.85|d_{zx}\rangle$, $|\psi_{A_2}\rangle = 0.38|d_{xy}\rangle - 0.85|d_{yz}\rangle + 0.35|d_{zx}\rangle$ and $|\psi_{B_2}\rangle = -0.71|d_{xy}\rangle + 0.71|d_{zx}\rangle$. This lattice distortion brings about new terms D'^l and E^l in the Hamiltonian (see the Appendix) which promote a mixing of the different kinds of orbitals. Thus, the uniform components of the orbital increase and the hopping integral between the occupied orbitals τ_{ij} becomes finite. As a result, the ferromagnetic ordering is relatively unstable in comparison with the AF spin ordering due to the term A^l. (2) The large JT distortion with the E_g symmetry $g_E Q_E$ favors the orbital ordered state of any linear combinations of the d_{xy} and d_{zx} orbitals for A_1 and A_2 sites, and those of the d_{xy} and d_{yz} orbitals for B_1 and B_2 sites. On the contrary, $g_{T_2} Q_{T_2}$ lifts the degeneracy uniquely as $|\psi_{A_1}\rangle = (1/\sqrt{2})(|d_{xy}\rangle - |d_{zx}\rangle)$, $|\psi_{A_2}\rangle = (1/\sqrt{2})(|d_{xy}\rangle + |d_{zx}\rangle)$, $|\psi_{B_1}\rangle = (1/\sqrt{2})(|d_{xy}\rangle + |d_{yz}\rangle)$, and $|\psi_{B_2}\rangle = (1/\sqrt{2})(|d_{xy}\rangle - |d_{yz}\rangle)$. The obtained orbital state in the F spin phase in Fig. 4(b) is the mixed state of the two. Here, the hopping integrals τ_{ij}'s become finite for all NN bonds. Thus, a region of the ferromagnetic phase shrinks by introducing gQ. (3) The LS coupling fixes the direction of spins in the ferromagnetic phase along [100]. The large orbital degeneracy at $\lambda_{\mathrm{LS}} = 0$ is lifted and one of the obtained orbital state is given by $|\psi_{A_1}\rangle = |\psi_{B_2}\rangle = (1/\sqrt{2})(i|d_{yz}\rangle + |d_{zx}\rangle)$ and $|\psi_{A_2}\rangle = |\psi_{B_1}\rangle = |d_{xy}\rangle$. Although this orbital ordered state is included in the solutions at $\lambda_{\mathrm{LS}} = 0$ shown in Eq. (30), there is no energy gain for the LS coupling at sites A_2 and B_1. This is because the F spin state is not compatible with the staggered orbital ordered state in the large limit of λ_{LS}.

IV. RESONANT X-RAY SCATTERING

RXS was first applied to observation of the orbital ordering in perovskite manganites.[31] By tuning the incident x-ray

energy to the K edge of the transition-metal ion, the atomic scattering factor becomes a tensor with respect to the polarization of x ray and is sensitive dramatically to the local electronic structure.[32] In this section, the scattering cross section of RXS in titanates is formulated. This is applied to the recent experimental results in $YTiO_3$. Let us consider the scattering of x ray with momentum $\vec{k}_i$, energy ω_i, and polarization λ_i to $\vec{k}_f, \omega_f$, and λ_f. The electronic states at the initial, final and intermediate states of the scattering are denoted by $|i\rangle, |f\rangle$, and $|m\rangle$ with energies $\varepsilon_i, \varepsilon_f$, and ε_m, respectively. We start with the conventional form for the differential scattering cross section of RXS (Refs. 33,32)

$$\frac{d^2\sigma}{d\Omega d\omega_f} = A\frac{\omega_f}{\omega_i}\sum_{|f\rangle} |S|^2 \delta(\varepsilon_f + \omega_f - \varepsilon_i - \omega_i), \tag{37}$$

where

$$S = \sum_m \left\{ \frac{\langle f|\vec{j}_{-k_i}\cdot\vec{e}_{k_i\lambda_i}|m\rangle\langle m|\vec{j}_{k_f}\cdot\vec{e}_{k_f\lambda_f}|i\rangle}{\varepsilon_i - \varepsilon_m - \omega_f} + \frac{\langle f|\vec{j}_{k_f}\cdot\vec{e}_{k_f\lambda_f}|m\rangle\langle m|\vec{j}_{-k_i}\cdot\vec{e}_{k_i\lambda_i}|i\rangle}{\varepsilon_i - \varepsilon_m + \omega_i + i\Gamma} \right\}, \tag{38}$$

with the cross section of the Thomson scattering $A = (e^2/mc^2)^2$. Γ denotes the damping of a core hole, $\vec{e}_{k\lambda}$ is the polarization vector of x ray, and $\vec{j}_k$ is the current operator. This form is rewritten by using the correlation function of the polarizability $\alpha_{l\beta\alpha}$ as shown in Ref. 34:

$$\frac{d^2\sigma}{d\Omega d\omega_f} = A\frac{\omega_f}{\omega_i}\sum_{\alpha\beta\alpha'\beta'} P_{\beta'\alpha'}P_{\beta\alpha}\Pi_{\beta'\alpha'\beta\alpha}(\omega,\vec{K}), \tag{39}$$

where

$$\Pi_{\beta'\alpha'\beta\alpha}(\omega,\vec{K}) = \frac{1}{2\pi}\int dt e^{i\omega t}\sum_{ll'} e^{-i\vec{K}\cdot(\vec{r}_{l'}-\vec{r}_l)} \times \langle i|\alpha_{l'\beta'\alpha'}(t)^\dagger \alpha_{l\beta\alpha}(0)|i\rangle, \tag{40}$$

with $\vec{K} = \vec{k}_i - \vec{k}_f, \omega = \omega_i - \omega_f$ and $P_{\beta\alpha} = (\vec{e}_{k_f\lambda_f})_\beta (\vec{e}_{k_i\lambda_i})_\alpha$. Now we express the polarizability operator by the orbital operators $O_{l\Gamma\gamma}$ by utilizing the group theoretical analyses. $\alpha_{l\beta\alpha}$ associated with the orbital operators at site l is represented by

$$\alpha_{l\beta\alpha}(t) = \sum_{\Gamma\gamma} I_\Gamma (M_{\Gamma\gamma})_{\beta\alpha} O_{l\Gamma\gamma}(t), \tag{41}$$

with $(\Gamma\gamma) = (Eu,Ev),(T_1x,T_1y,T_1z)$, and (T_2x,T_2y,T_2z). I_Γ's are coupling constants which are not determined by the group theoretical analyses and $M_{\Gamma\gamma}$'s are matrices with respect to the polarization of x ray. Explicit forms of $M_{\Gamma\gamma}$ are given by the Gell-Mann matrices λ_l introduced in Sec. II as $M_{\Gamma\gamma} = \lambda_l$ for $(\Gamma\gamma;l) = (Eu;8),(Ev,3), M_{\Gamma\gamma} = -\lambda_l$ for $(T_2x;6),(T_2y;4),(T_2z;1)$, and $M_{\Gamma\gamma} = -i\lambda_l$ for $(T_1x;7),(T_1y;5),(T_1z;2)$. As a result, the cross section for the static scattering in the orbital ordered state is obtained as

$$\frac{d\sigma}{d\Omega} = \frac{A}{2\pi}N^2|B(\vec{K})|^2, \tag{42}$$

with

$$B(\vec{K}) = \sum_{\Gamma\gamma} I_{\Gamma\gamma} S_{\Gamma\gamma} \langle O_{\Gamma\gamma}(\vec{K})\rangle. \tag{43}$$

Here, $S_{\Gamma\gamma}$ is the polarization part of the cross section defined by

$$S_{\Gamma\gamma} = \vec{e}^{\,t}_{k_f\lambda_f} M_{\Gamma\gamma} \vec{e}_{k_i\lambda_i}, \tag{44}$$

and $\langle O_{\Gamma\gamma}(\vec{K})\rangle$ is the orbital order parameter

$$\langle O_{\Gamma\gamma}(\vec{K})\rangle = \frac{1}{N}\sum_l e^{i\vec{K}\cdot\vec{r}_l}\langle O_{l\Gamma\gamma}\rangle, \tag{45}$$

with a number of the unit cell N. Equation (42) with Eq. (43) is derived by only considering the symmetries of crystal and orbital. Therefore, we do not specify, in this paper, the microscopic origin of the orbital dependence of the polarizability. However, it is reported recently that the mechanism of RXS based on the Coulomb interactions between $3d$ and $4p$ electrons well explains relative scattering intensities at different reflection points in $YTiO_3$, rather than the mechanism based on the lattice distortions.[22,35]

The above results are applied to RXS in $YTiO_3$ where the detailed experiments have been done recently and reported in Ref. 22. In the RXS experiments, the azimuthal angle scan, which is the rotational scan about the scattering vector $\vec{K}$, is crucially important to identify the orbital ordering.[31] This is because the local symmetry of the orbital structure directly reflects on the azimuthal angle dependence. A schematic picture of the experimental arrangement is presented in the inset of Fig. 5(a). In this arrangement, $S_{\Gamma\gamma}$ in Eq. (42) is replaced by

$$S_{\Gamma\gamma} = \vec{e}^{\,t}_{k_f\lambda_f} U(\varphi) V M_{\Gamma\gamma} V^{-1} U^{-1}(\varphi) \vec{e}_{k_i\lambda_i}, \tag{46}$$

where the matrix V describes the transformation from the crystallographic coordinate to the laboratory coordinate and the matrix $U(\varphi)$ represents the azimuthal rotation with the rotation angle φ. The $GdFeO_3$-type lattice distortion is also taken into account. A general formalism for the azimuthal angle dependence of RXS intensity is presented in Ref. 36. The RXS experiments have been carried out at three orbital superlattice reflection points of (100),(001), and (011), where we use the $Pbnm$ orthorhombic notations. We fit the four sets of the experimental data: (100) with $(\lambda_i,\lambda_f) = (\sigma,\pi)$,(001) with (σ,π),(011) with (σ,σ), and (011) with (σ,π), where $\sigma(\pi)$ indicates the $\sigma(\pi)$ polarization of x ray. From now on, the scattering intensity at (hkl) with polarizations (λ_i,λ_f) is denoted by $I(hkl)_{\lambda_i\lambda_f}$. $I(100)_{\sigma\sigma}$ and $I(001)_{\sigma\sigma}$ are zero within the experimental errors. We assume that the orbital wave functions have a symmetry of the $Pbnm$ point group. Then, the coefficients $C_{i\alpha}$ in the orbital wave functions [see Eq. (28)] satisfy the conditions

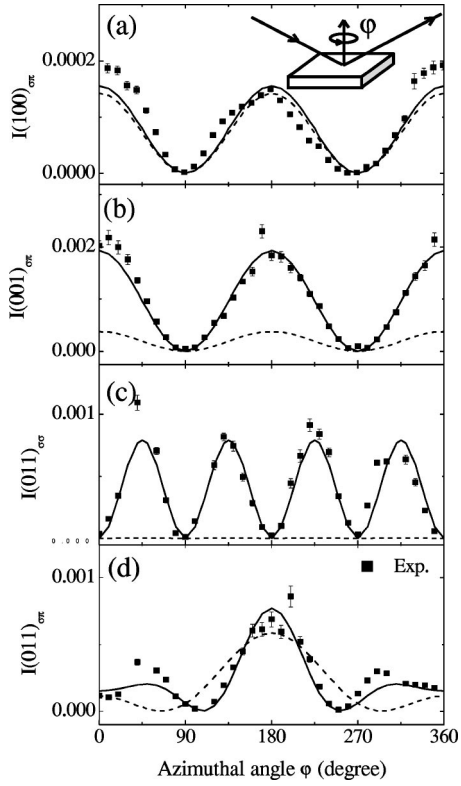

FIG. 5. The azimuthal angle dependence of the resonant x-ray scattering intensity. (a) $I(100)_{\sigma\pi}$, (b) $I(001)_{\sigma\pi}$, (c) $I(011)_{\sigma\sigma}$, and (d) $I(011)_{\sigma\pi}$. The bold curves show the fitted results by the wave functions $(a,b,c)=(-0.71,\ 0,\ 0.71)$. The doted curves show the calculated results by the wave functions $(a,b,c)=(1/\sqrt{2},0,i/\sqrt{2})$. The filled squares indicate the experimental data in $YTiO_3$ normalized by the intensity at (022) obtained in Ref. 22. The inset of (a) shows a schematic picture of experimental arrangement.

$C_{A_1yz}=C_{A_2yz}=C_{B_1zx}=C_{B_2zx}\equiv a$, $C_{A_1zx}=C_{A_2zx}=C_{B_1yz}=C_{B_2yz}\equiv b$, and $C_{A_1xy}=-C_{A_2xy}=C_{B_1xy}=-C_{B_2xy}\equiv c$. In the case where *a*, *b* and *c* are real, the explicit forms of the scattering intensities are given by

$$I(100)_{\sigma\sigma}=0, \tag{47}$$

$$I(100)_{\sigma\pi}=I_0(4I_E O_{Ev}\sin\varphi\cos\theta)^2, \tag{48}$$

$$I(001)_{\sigma\sigma}=0, \tag{49}$$

$$I(001)_{\sigma\pi}=I_0(4I_{T_2}O_{T_2}\sin\varphi\cos\theta)^2, \tag{50}$$

$$I(011)_{\sigma\sigma}=I_0 8(I_{T_2}O_{T_2}\sin 2\varphi)^2, \tag{51}$$

$$I(011)_{\sigma\pi}=I_0 8(I_{T_2}O_{T_2})^2(-\cos 2\varphi\sin\theta+\sin\varphi\cos\theta)^2, \tag{52}$$

where the $GaFeO_3$-type distortion is neglected. θ is the scattering angle, $I_0=AN^2/(2\pi)$ and, O_{Ev} and O_{T_2} are the order parameters given by

$$O_{Ev}=\langle O_{A_1Ev}\rangle=\frac{1}{\sqrt{2}}(a^2-b^2) \tag{53}$$

and

$$O_{T_2}=\frac{1}{2}(\langle O_{A_1T_2x}\rangle-\langle O_{A_2T_2y}\rangle)=\frac{1}{\sqrt{2}}c(a-b), \tag{54}$$

respectively. It is worth mentioning that $I(100)_{\sigma\pi}$ and other I's are reflected from different components of the orbital order parameters, i.e., O_{Ev} and O_{T_2}, respectively. From the above considerations, a,b, and c are restricted so that c is finite and $a\neq b$. We optimize values of a,b,c and I_{T_2}/I_E numerically within real numbers. It is found that the calculated results fit in the four sets of the experimental data simultaneously, when the wave function (a,b,c) satisfies the condition $c\gtrsim -a\gg|b|$. One of the best fitted results is obtained by a set of the parameters $(a,b,c)=(-0.71,\ 0,\ 0.71)$ being consistent with the recent experimental analyses,[22,17] and $I_{T_2}/I_E=0.45$. The results are shown in Fig. 5 (bold lines) together with the experimental data (filled squares). The fitting by the calculation is satisfactory. For comparison, we calculate the RXS intensity where the orbital wave functions are complex (dotted lines in Fig. 5). We set $a=1/\sqrt{2},b=0$ and $c=i/\sqrt{2}$. In this case, the scattering intensities are explicitly given by

$$I(100)_{\sigma\pi}=I_0(4I_E O_{Ev}\sin\varphi\cos\theta)^2, \tag{55}$$

$$I(001)_{\sigma\pi}=I_0(I_{T_1}O_{T_1}\sin\varphi\cos\theta)^2, \tag{56}$$

$$I(011)_{\sigma\pi}=I_0\frac{1}{2}(I_{T_1}O_{T_1})^2(\sin\theta+\sin\varphi\cos\theta)^2, \tag{57}$$

and $I_{\sigma\sigma}$'s are zero. O_{T_1} is the order parameter for the magnetic dipole moment defined by

$$O_{T_1}=\langle O_{A_1T_1x}\rangle=\frac{i}{\sqrt{2}}(a^*c-c^*a). \tag{58}$$

The discrepancies between the calculated results and the experimental data are remarkable, especially, in $I(011)_{\sigma\sigma}$. This is because the order parameter O_{T_2} vanishes and O_{T_1} appears in this orbital ordered state.

By using the orbital wave function $(a,b,c)=(-0.71,\ 0,\ 0.71)$ obtained above, the spin wave dispersion relation is calculated by applying the Holstein-Primakoff transformation. The results are presented in Fig. 6 for several values of R_t. In the same sets of parameters, the Curie temperature T_C is calculated by the mean-field approximation, and calculated values are corrected by considering the results in the high temperature expansion.[37] $R_D=D_{zz}/D_{xy}$, where $D_{zz}(D_{xy})$ is the spin stiffness in the z direction (the xy plane), and T_C is obtained as $(R_D,T_C/J_{T_1})=(0.75,0.21),(1.00,0.25),(1.23,0.30)$ for $R_t=0.74,0.84,0.94$, respectively. The spin wave in $YTiO_3$ is recently measured in Ref. 38 by neutron scattering experi-

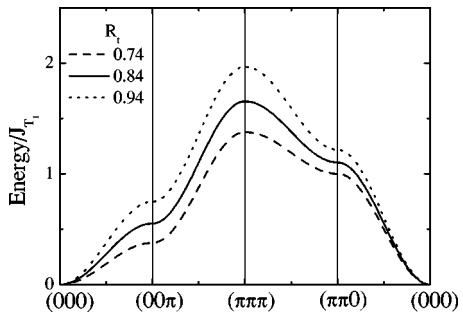

FIG. 6. The dispersion relation of the spin wave. Broken, bold, and dotted curves are the results with $R_t=0.74,0.84$, and 0.94, respectively. The cubic notation is used. The orbital wave functions are chosen as $(a,b,c)=(-0.71,0,0.71)$, and R_J is fixed to be 0.25. The ratio of the spin wave stiffness constant $R_D=D_{zz}/D_{xy}$ and the Curie temperature T_C is $(R_D,T_C/J_{T_1})=(0.75,0.21),(1.00,0.25),(1.23,0.30)$ for $R_t=0.74,0.84$, and 0.94, respectively.

ments and its dispersion relation is found to be almost isotropic. A value of J_{T_1} is estimated by fitting the experimental data by the calculated results of $R_t=0.84$ where the spin stiffness is almost isotropic. The obtained value is $J_{T_1}=10.9$ meV by which T_C is given by 32 K. This result is consistent with T_C in $YTiO_3$ of about 30 K.

V. SUMMARY

In summary, we derive the effective Hamiltonian for spin and orbital states in perovskite titanates $R_{1-x}A_xTiO_3$. By taking into account the threefold orbital degeneracy, the orbital parts of the Hamiltonian are represented by the eight 3×3 matrices. The orbital ordered states in the ferromagnetic phase for the end compounds have strong continuous degeneracy. This is owing to the threefold degenerated t_{2g} orbitals and the orthogonality of the electron hopping integral between NN ions, unlike the twofold degenerated e_g orbitals. Introductions of the $GdFeO_3$-type distortion, the JT-type distortion and the LS coupling lift the orbital degeneracy and destabilize the ferromagnetic state. This implies that the high symmetry in the orbital space is favored for the ferromagnetic ordering. The scattering cross section of RXS is formulated by utilizing the same orbital operators adopted in the Hamiltonian. It is shown that the different components of the orbital order parameters are detected separately at the different reflection points and polarization configurations. The experimental data of the azimuthal angle dependent RXS intensities are well fitted by the present calculation.

The present theory based on the derived effective Hamiltonian and new RXS formula is satisfactory to explain the several experiments about spin and orbital states in $YTiO_3$. It is thought that the spin and orbital states are controlled by the interactions between NN Ti sites through the virtual electron exchange processes and the associated JT-type lattice distortions. The present RXS studies suggest that the LS coupling may be irrelevant and the real orbital wave functions are realized by the inter-site interaction between orbitals.

Beyond the static spin and orbital ordered states in $RTiO_3$, this Hamiltonian is applicable to the orbital excitations termed orbital wave[24] and to the hole doped systems $R_{1-x}A_xTiO_3$. For the actual calculations, the present Hamiltonian represented by the 3×3 matrices $O_{i\Gamma\gamma}$ is more convenient than that by the 2×2 matrices T_{il} [see Eq. (22)] with the constraint and the Hubbard type Hamiltonian. The study of the doped titanates and the orbital dynamics will be presented in a separate publication.

ACKNOWLEDGMENTS

The authors would like to thank Y. Murakami, H. Nakao, D. Gibbs, and J.P. Hill for providing their experimental data prior publication. The authors also appreciate the valuable discussions with G. Khaliullin and B. Keimer. This work was supported by the Grant in Aid from Ministry of Education, Culture, Sports, Science and Technology of Japan, CREST, and Science and Technology Special Coordination Fund for Promoting Science and Technology. One of authors (S.M.) acknowledges support of the Hunboldt Foundation.

APPENDIX: EFFECTIVE HAMILTONIAN WITH A $GdFeO_3$-TYPE LATTICE DISTORTION

Effects of the $GdFeO_3$-type lattice distortion are included in the modified J term $\tilde{\mathcal{H}}_J$ introduced in Eq. (34). The explicit form of this term is given by

$$\tilde{\mathcal{H}}_J=\mathcal{H}_J+\tilde{\mathcal{H}}_{T_1}+\tilde{\mathcal{H}}_{T_2}+\tilde{\mathcal{H}}_E+\tilde{\mathcal{H}}_{A_1}, \tag{A1}$$

with

$$\tilde{\mathcal{H}}_{T_1}=-J_{T_1}\sum_{\langle ij\rangle}\left(\frac{3}{4}+\vec{S}_i\cdot\vec{S}_j\right)\left\{s_l R_t 2D'^l+R_t^2\left(\frac{1}{2}A^l-C'^l+D^l\right)\right\}, \tag{A2}$$

$$\tilde{\mathcal{H}}_{T_2}=-J_{T_2}\sum_{\langle ij\rangle}\left(\frac{1}{4}-\vec{S}_i\cdot\vec{S}_j\right)\left\{s_l R_t 2(D'^l+E'^l)+R_t^2\left(\frac{1}{2}A^l+C'^l+D^l\right)\right\}, \tag{A3}$$

$$\tilde{\mathcal{H}}_E=-J_E\sum_{\langle ij\rangle}\left(\frac{1}{4}-\vec{S}_i\cdot\vec{S}_j\right)\left\{s_l R_t\frac{2}{3}E^l+R_t^2\left(\frac{4}{3}B^l-\frac{2}{3}C^l\right)\right\}, \tag{A4}$$

$$\tilde{\mathcal{H}}_{A_1}=-J_{A_1}\sum_{\langle ij\rangle}\left(\frac{1}{4}-\vec{S}_i\cdot\vec{S}_j\right)\left\{s_l R_t\frac{4}{3}E^l+R_t^2\left(\frac{2}{3}B^l+\frac{2}{3}C^l\right)\right\}. \tag{A5}$$

The parameter $R_t=t_\sigma/t_\pi$ is caused by the $GdFeO_3$-type distortion. A^l, B^l, C^l, C'^l, and D^l are defined in Eqs. (16), (17), (18), (19), and (20), respectively. D'^l and E^l describe new exchange processes induced by the distortion and are given by

$$D' = -\sqrt{2}\left(\frac{1}{3}+\sqrt{\frac{2}{3}}O^l_{iEu}\right)O_{jT_2l}-\sqrt{2}O_{iT_2l}\left(\frac{1}{3}+\sqrt{\frac{2}{3}}O^l_{jEu}\right), \tag{A6}$$

$$E^l = -\sqrt{2}\left(\frac{2}{3}-\sqrt{\frac{2}{3}}O^l_{iEu}\right)O_{jT_2l}-\sqrt{2}O_{iT_2l}\left(\frac{2}{3}-\sqrt{\frac{2}{3}}O^l_{jEu}\right). \tag{A7}$$

By utilizing the pseudospin operator introduced in Eq. (22), these terms are rewritten as

$$D' = 2(n_{ic_l}T^l_{jx}+T^l_{ix}n_{jc_l}), \tag{A8}$$

$$E^l = 2\{(n_{ia_l}+n_{ib_l})T^l_{jx}+T^l_{ix}(n_{ja_l}+n_{jb_l})\}. \tag{A9}$$

[1] See, for a review, M. Imada, A. Fujimori, and Y. Tokura, Rev. Mod. Phys. **70**, 1039 (1998).
[2] D.A. MacLean, H.-N. Ng, and J.E. Greedan, J. Solid State Chem. **30**, 35 (1979).
[3] J.P. Goral, J.E. Greedan, and A.D. MacLean, J. Solid State Chem. **43**, 244 (1982).
[4] D.A. MacLean and J.E. Greedan, Inorg. Chem. **20**, 1025 (1981).
[5] J.D. Garrett, J.E. Greedan, and D.A. MacLean, Mater. Res. Bull. **16**, 145 (1981).
[6] T. Arima, Y. Tokura, and J.B. Torrance, Phys. Rev. B **48**, 17 006 (1993); T. Arima, and Y. Tokura, J. Phys. Soc. Jpn. **64**, 2488 (1995).
[7] Y. Taguchi, Y. Tokura, T. Arima, and F. Inaba, Phys. Rev. B **48**, 511 (1993).
[8] A. Fujimori, I. Hase, H. Namatame, Y. Fujishima, Y. Tokura, H. Eisaki, S. Uchida, K. Takegahara, and F.M.F. de Groot, Phys. Rev. Lett. **69**, 1796 (1992).
[9] Y. Tokura, Y. Taguchi, Y. Okada, Y. Fujishima, T. Arima, K. Kumagai, and Y. Iye, Phys. Rev. Lett. **70**, 2126 (1993).
[10] Y. Tokura, Y. Taguchi, Y. Moritomo K. Kumagai, T. Suzuki, and Y. Iye, Phys. Rev. B **48**, 14 063 (1993).
[11] T. Katsufuji, Y. Okimoto, and Y. Tokura, Phys. Rev. Lett. **75**, 3497 (1995).
[12] See, for a review, Y. Tokura and N. Nagaosa, Science **288**, 462 (2000).
[13] T. Mizokawa and A. Furjimori, Phys. Rev. B **54**, 5368 (1996); T. Mizokawa, D.I. Khomskii, and G.A. Sawatzky, *ibid.* **60**, 7309 (1999).
[14] H. Sawada, N. Hamada, and K. Terakura, Physica B **237-238**, 46 (1997); H. Sawada and K. Terakura, Phys. Rev. B **58**, 6831 (1998).
[15] S. Okubo, S. Kimura, H. Ohta, and M. Itoh, J. Magn. Magn. Mater. **177-181**, 1373 (1998).
[16] M. Itoh, M. Tsuchiya, H. Tanaka, and K. Motoya, J. Phys. Soc. Jpn. **68**, 2783 (1999).
[17] H. Ichikawa, J. Akimitsu, M. Nishi, and K. Kakurai, Physica B **281&282**, 482 (2000).
[18] B. Keimer, D. Casa, A. Ivanov, J.W. Lynn, M.v. Zimmermann, J.P. Hill, D. Gibbs, Y. Taguchi, and Y. Tokura, Phys. Rev. Lett. **85**, 3946 (2000).
[19] G. Khaliullin and S. Maekawa, Phys. Rev. Lett. **85**, 3950 (2000).
[20] M. Mochizuki and M. Imada, J. Phys. Soc. Jpn. **69**, 1982 (2000); cond-mat/0105135 (unpublished).
[21] M. Mochizuki and M. Imada, cond-mat/0102223 (unpublished).
[22] H. Nakao, Y. Wakabayashi, T. Kiyama, Y. Murakami, M. v. Zimmermann, J. P. Hill, D. Gibbs, S. Ishihara, Y. Taguchi, and Y. Tokura (unpublished); Bull. Am. Phys. Soc. **46**, 250 (2001).
[23] F.C. Zhang and T.M. Rice, Phys. Rev. B **37**, 3759 (1988).
[24] S. Ishihara, J. Inoue, and S. Maekawa, Physica C **263**, 130 (1996); Phys. Rev. B **55**, 8280 (1997).
[25] A.E. Bocquet, T. Mizokawa, K. Morikawa, A. Fujimori, S.R. Barman, K. Maiti, D.D. Sarma, Y. Tokura, and M. Onoda, Phys. Rev. B **53**, 1161 (1996).
[26] M. Gell-Mann and Y. Ne'eman, *The Eightfold Way* (Benjamin, New York, 1964).
[27] K.I. Kugel and D.I. Khomskii, Sov. Phys. Solid State **17**, 285 (1975).
[28] K.I. Kugel, and D.I. Khomskii, Sov. Phys. JETP **37**, 725 (1973).
[29] S. Ishihara and S. Maekawa, Phys. Rev. B **62**, 2338 (2000).
[30] J.C. Slater and G.F. Koster, Phys. Rev. **94**, 1498 (1954).
[31] Y. Murakami, H. Kawada, H. Kawata, M. Tanaka, T. Arima, H. Moritomo, and Y. Tokura, Phys. Rev. Lett. **80**, 1932 (1998).
[32] S. Ishihara and S. Maekawa, Phys. Rev. Lett. **80**, 3799 (1998).
[33] M. Blume, J. Appl. Phys. **57**, 3615 (1985).
[34] S. Ishihara and S. Maekawa, Phys. Rev. B **62**, R9252 (2000).
[35] M. Takahashi and J. Igarashi, cond-mat/0104480 (unpublished) .
[36] S. Ishihara and S. Maekawa, Phys. Rev. B **58**, 13 442 (1998).
[37] C. Domb and M.F. Sykes, Proc. R. Soc. London, Ser. A **240**, 214 (1957).
[38] C. Ulrich, H. He, G. Khaliullin, J.W. Lynn, A. Ivanov, M. Ohl, Y. Taguchi, Y. Tokura, and B. Keimer, Bull. Am. Phys. Soc. **46**, 1175 (2001).